Communication

Wave Diffraction by Metamaterial-Coated Wedges: The UAPO Solution for Skew Incidence

Giovanni Riccio [1,*] , **Gianluca Gennarelli** [2] , **Flaminio Ferrara** [3] , **Claudio Gennarelli** [3] **and Rocco Guerriero** [3]

[1] D.I.E.M., University of Salerno, Via Giovanni Paolo II, 132, 84084 Fisciano, SA, Italy
[2] IREA-CNR, Via Diocleziano, 328, 80124 Naples, NA, Italy
[3] D.I.In., University of Salerno, Via Giovanni Paolo II, 132, 84084 Fisciano, SA, Italy
[*] Correspondence: griccio@unisa.it

Abstract: The interaction between an electromagnetic plane wave and a metallic wedge coated with a uniform layer made of a double-negative metamaterial is studied by means of the uniform asymptotic physical optics method in the high-frequency range, e.g., at microwave and optical frequencies. The apex angle of the structure is arbitrarily chosen, and the wave is at a skew incidence with respect to the external edge, which is formed by the metamaterial layers covering the wedge faces. The proposed method is built on the scattering integral involving electric and magnetic surface currents as physical optics equivalent sources, and it takes advantage of analytic evaluations. The last step uses a uniform asymptotic procedure to obtain a closed form expression of the diffracted field to be added to the geometrical optics one for computing the total field at the observation point in the neighboring free space. The study also includes a numerical validation of the method.

Keywords: diffraction; wedge; metamaterial

1. Introduction

The electromagnetic scattering involving a perfect electric conducting (PEC) wedge with arbitrary apex angle and uniform coating by a double-negative metamaterial (DNG MTM) with losses has been tackled in [1,2] by considering an incident plane wave that is perpendicular to the edge. This two-dimensional problem has been studied at high frequencies by applying the Uniform Asymptotic Physical Optics (UAPO) method in the framework of the Uniform Geometrical Theory of Diffraction (UTD) [3], which gives a very attractive model that combines the diffraction contribution and the Geometrical Optics (GO) ones for the scattering computation. In the UAPO method, the electric and magnetic surface currents have been used as equivalent sources on the external surfaces of the composite structure and incorporated in the scattering integral. Closed-form expressions have been obtained for parallel and perpendicular polarizations with respect to the edge of the structure by adopting useful approximations and integral representations, and performing asymptotic evaluations of the resulting integrals. The capability of the UAPO diffracted field to balance the GO field at the shadow boundaries has been demonstrated by means of numerical tests [1,2].

The solution for the two-dimensional plane wave diffraction in [1,2], as well as that which was proposed in [4], has an application that is limited to schemes concerning normal incidences. Accordingly, the UAPO solution for the three-dimensional scenario of plane waves at a skew incidence is needed.

This article addresses the above need by accounting for the relevance of scattering problems involving coated metallic wedges, the metallic part of which can be replaced by a PEC structure with the same geometry at high frequencies, where the UAPO approach works. As it is well known, the electromagnetic scattering of dielectric and metallic structures can be modified by adding layers on their surfaces, and therefore such a practice results very attractive for civil and military applications, i.e., airplanes and ships can necessitate to

lower their radar cross section by covering the metallic surfaces. Moreover, metamaterials have been recently proposed in Intelligent Reflecting Surfaces (IRS). This article refers to a particular structure that can be allocated in a smart wireless propagation scenario. The unusual electromagnetic peculiarities of DNG MTMs are related to the negative real parts of their permittivity and permeability, and offer unconventional solutions with respect to the standard materials, so opening new frontiers for research activities and applications. The reader that is fascinated by such materials can find interesting information and applications, as well as available manufacturing processes, in several books and articles (see [5–12] also for help in finding other references).

The UAPO approach has been already applied to solve three-dimensional scattering problems. A planar junction between a double-positive material and a DNG MTM with a PEC backing has been considered in [13], whereas the scattering by a structure that is formed by a truncated DNG MTM sheet accommodated on a PEC support has been studied in [14]. Some references [15–20] contain solutions for the plane wave diffraction problems involving dielectric wedges. In particular, the time domain counterpart of the UAPO solution in [19] has been obtained in [20] with reference to a penetrable wedge, which has an acute apex angle. The corresponding UAPO diffracted field has been always formulated in explicit and easy-to-use forms, and the effectiveness of the solutions has been demonstrated by adopting well-assessed numerical tools.

As pointed out in a previous statement, the UAPO method is applied in this article for solving the three-dimensional scattering problem of obliquely incident plane waves, which illuminate a PEC wedge with a DNG MTM planar coating. Since the method requires the evaluation of the field, which is reflected from the structure, the reflection coefficients need to be evaluated for each wedge surface that is involved in the scattering mechanism. The equivalent transmission line (ETL) model is here applied to this purpose in accordance with [1,2,13,20], and the results are used to formulate the PO currents on the surfaces. Opportune approximations, analytical manipulations and evaluations, and the application of an asymptotic procedure permit us to extract the UAPO diffracted contribution from the scattering integral part that is associated with each wedge surface if this last is lit by the incident plane wave. In other words, each surface contributes to the diffracted field only if it interacts with the propagating plane wave.

Section 2 is devoted to the formulation of the PO equivalent surface currents incorporating the reflection coefficients that are related to each wedge surface, whereas the UAPO solution for the diffracted field is proposed in Section 3. The radio frequency (RF) unit of Comsol Multiphysics® is applied in Section 4 to test the efficacy of the proposed approach. The conclusions are presented in Section 5.

2. PO Equivalent Surface Currents

A DNG MTM uniform layer with thickness d, permittivity $\varepsilon = \varepsilon_0 \varepsilon_r = -\varepsilon_0(\varepsilon' + j\varepsilon'')$ and permeability $\mu = \mu_0 \mu_r = -\mu_0(\mu' + j\mu'')$, where $\varepsilon', \varepsilon'', \mu', \mu''$ are positive quantities and ε_0, μ_0 are related to the free space, covers an arbitrary-angled metallic wedge that is assumed to be PEC at the working frequencies and to have an apex angle $\alpha = (2 - n)\pi$.

According to Figure 1, the external surface $S = S_0 \cup S_{n\pi}$ of the wedge is lit by an incident plane wave with the electric field $\underline{E}^i = \underline{E}^i_0 \exp(-j\underline{k}^i \cdot \underline{r})$, where $\underline{k}^i = k_0 \hat{\underline{k}}^i$ (k_0 is the free-space propagation constant) and the vector $\underline{r}$ locates the observation point P. If the PO approximation holds, such a field generates the following electric $\left(\underline{J}_s \right)$ and magnetic $\left(\underline{M}_s \right)$ equivalent surface currents on S_0 and $S_{n\pi}$:

$$\underline{J}\bigg|_{S_{0,n\pi}} = \hat{n}_{0,n\pi} \times (\underline{H}^i + \underline{H}^r)\bigg|_{S_{0,n\pi}} =$$

$$= \left[(1 - R_{\perp_{0,n\pi}})E^i_{\perp_{0,n\pi}}\cos\theta^i_{0,n\pi}\hat{u}_{\perp_{0,n\pi}} + (1 + R_{\parallel_{0,n\pi}})E^i_{\parallel_{0,n\pi}}(\hat{n}_{0,n\pi} \times \hat{u}_{\perp_{0,n\pi}})\right]\frac{\exp(-j\underline{k}^i\cdot\underline{r}'_{0,n\pi})}{\zeta_0} \qquad (1)$$

$$\underline{M}\bigg|_{S_{0,n\pi}} = (\underline{E}^i + \underline{E}^r)\bigg|_{S_{0,n\pi}} \times \hat{n}_{0,n\pi} =$$

$$= \left[(1 - R_{\parallel_{0,n\pi}})E^i_{\parallel_{0,n\pi}}\cos\theta^i_{0,n\pi}\hat{u}_{\perp_{0,n\pi}} - (1 + R_{\perp_{0,n\pi}})E^i_{\perp_{0,n\pi}}(\hat{n}_{0,n\pi} \times \hat{u}_{\perp_{0,n\pi}})\right]\exp(-j\underline{k}^i\cdot\underline{r}'_{0,n\pi}). \qquad (2)$$
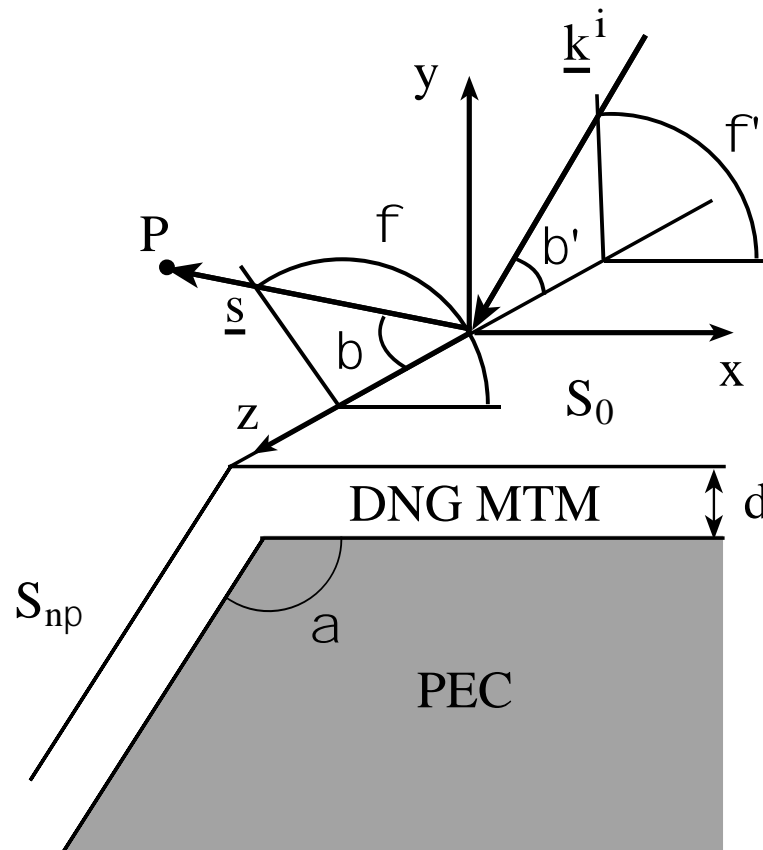

Figure 1. The diffraction problem.

In the above expressions, $\zeta_0 = \sqrt{\mu_0/\varepsilon_0}$, the symbols $\parallel$ and $\perp$ refer to parallel and perpendicular polarizations, respectively, $\hat{n}_{0,n\pi}$ is the unit vector normal to the involved surface, $\hat{u}_{\perp_{0,n\pi}} = (\hat{k}^i \times \hat{n}_{0,n\pi})\big/\left|\hat{k}^i \times \hat{n}_{0,n\pi}\right|$, and $\cos\theta^i_{0,n\pi} = -\hat{k}^i \cdot \hat{n}_{0,n\pi}$. The ETL model is applied to calculate the reflection coefficients R:

$$R_{\parallel,\perp_{0,n\pi}} = \frac{Z^{in}_{\parallel,\perp_{0,n\pi}} - Z^0_{\parallel,\perp_{0,n\pi}}}{Z^{in}_{\parallel,\perp_{0,n\pi}} + Z^0_{\parallel,\perp_{0,n\pi}}}, \qquad (3)$$

in which $Z^0_{\parallel_{0,n\pi}} = \zeta_0\cos\theta^i_{0,n\pi}$ and $Z^0_{\perp_{0,n\pi}} = \zeta_0/\cos\theta^i_{0,n\pi}$ are the free-space ETL characteristic impedances, and the ETL input impedances Z^{in} for a DNG MTM layer covering a PEC support can be evaluated according to [1,2,13,20].

Formulas (1) and (2) provide zero surface currents if the incident wave does not illuminate the corresponding surface.

3. UAPO Diffracted Field

The equivalent sources (1) and (2) are then assumed to radiate in the free space around the wedge, and the following integral formulation can be used to evaluate the scattered field $\underline{E}^s$ by accounting for the linearity of the integral operator:

$$
\begin{aligned}
\underline{E}^s = \ & -jk_0 U_0 \iint_{S_0} \left[\left(\underline{\underline{I}} - \hat{u}_0 \hat{u}_0 \right) \zeta_0 \underline{J}_{s_0} + \underline{M}_{s_0} \times \hat{u}_0 \right] G\left(\underline{r}, \underline{r}'_0 \right) dS + \\
& -jk_0 U_{n\pi} \iint_{S_{n\pi}} \left[\left(\underline{\underline{I}} - \hat{u}_{n\pi} \hat{u}_{n\pi} \right) \zeta_0 \underline{J}_{s_{n\pi}} + \underline{M}_{s_{n\pi}} \times \hat{u}_{n\pi} \right] G\left(\underline{r}, \underline{r}'_{n\pi} \right) dS,
\end{aligned}
\tag{4}
$$

where $G\left(\underline{r}, \underline{r}'_{0,n\pi} \right) = \exp\left(-jk_0 \left| \underline{r} - \underline{r}'_{0,n\pi} \right| \right) / \left(4\pi \left| \underline{r} - \underline{r}'_{0,n\pi} \right| \right)$ and $\hat{u}_{0,n\pi} = \left(\underline{r} - \underline{r}'_{0,n\pi} \right) / \left| \underline{r} - \underline{r}'_{0,n\pi} \right|$ account for the positions of P and the source points at $\underline{r}'_{0,n\pi}$. The term $\underline{\underline{I}}$ is the 3×3 identity matrix and $U_{0,n\pi}$ is equal to 1 if the related surface is lit by the incident plane wave or its value is 0.

The incidence direction $\hat{k}^i = -\cos\phi' \sin\beta' \hat{x} - \sin\phi' \sin\beta' \hat{y} + \cos\beta' \hat{z}$ is assumed (see Figure 1). According to [13,14], the UAPO approach is able to extract the diffraction contributions from (4) and to provide the diffracted field $\underline{E}^d$ at $P(s, \beta, \phi)$ with $\beta = \beta'$ (s symbolizes the distance from the diffraction point to P and ϕ varies from 0 to $n\pi$ on the arc of circumference with radius $\rho = s \sin\beta$ and center on the external edge):

$$
\begin{pmatrix} E_\beta^d \\ E_\phi^d \end{pmatrix} = \frac{\exp(-jk_0 s)}{\sqrt{s}} \left[U_0 F_0^d \underline{\underline{N}}_A + U_{n\pi} F_{n\pi}^d \underline{\underline{N}}_B \right] \begin{pmatrix} E_{\beta'}^i \\ E_{\phi'}^i \end{pmatrix} = \frac{\exp(-jk_0 s)}{\sqrt{s}} \underline{\underline{D}} \begin{pmatrix} E_{\beta'}^i \\ E_{\phi'}^i \end{pmatrix}.
\tag{5}
$$

Accordingly, the matrix $\underline{\underline{D}}$ of the diffraction coefficients is given by the superposition of the surface contributions and uses:

$$
F_0^d = \frac{\exp(-j\pi/4)}{2\sqrt{2\pi k_0}} \frac{F\left(2k_0 s \sin^2\beta' \cos^2\left(\frac{\phi'+\phi}{2} \right) \right)}{(\cos\phi' + \cos\phi) \sin^2\beta'}
\tag{6}
$$

$$
F_{n\pi}^d = \frac{\exp(-j\pi/4)}{2\sqrt{2\pi k_0}} \frac{F\left(2k_0 s \sin^2\beta' \cos^2\left(\frac{(n\pi - \phi') + (n\pi - \phi)}{2} \right) \right)}{\left[\cos(n\pi - \phi') + \cos(n\pi - \phi) \right] \sin^2\beta'}
\tag{7}
$$

$$
\underline{\underline{N}}_A = \underline{\underline{N}}_{A_1} \left[\underline{\underline{N}}_{A_2} \underline{\underline{N}}_{A_4} \underline{\underline{N}}_{A_5} + \underline{\underline{N}}_{A_3} \underline{\underline{N}}_{A_4} \underline{\underline{N}}_{A_6} \right] \underline{\underline{N}}_{A_7}
\tag{8}
$$

$$
\underline{\underline{N}}_B = \underline{\underline{N}}_{B_1} \left[\underline{\underline{N}}_{B_2} \underline{\underline{N}}_{B_4} \underline{\underline{N}}_{B_5} + \underline{\underline{N}}_{B_3} \underline{\underline{N}}_{B_4} \underline{\underline{N}}_{B_6} \right] \underline{\underline{N}}_{B_7}.
\tag{9}
$$

The function $F(\cdot)$ of the UTD model [3] is incorporated in (6) and (7). Furthermore,

$$
\underline{\underline{N}}_{A_1} = \begin{pmatrix} \cos\phi \cos\beta' & \sin\phi \cos\beta' & -\sin\beta' \\ -\sin\phi & \cos\phi & 0 \end{pmatrix}
\tag{10}
$$

$$
\underline{\underline{N}}_{A_2} = \begin{pmatrix} 1 - (\cos\phi \sin\beta')^2 & -\cos\phi \sin\beta' \cos\beta' \\ -\sin\phi \cos\phi \sin^2\beta' & -\sin\phi \sin\beta' \cos\beta' \\ -\cos\phi \sin\beta' \cos\beta' & \sin^2\beta' \end{pmatrix}
\tag{11}
$$

$$
\underline{\underline{N}}_{A_3} = \begin{pmatrix} 0 & -\sin\phi \sin\beta' \\ -\cos\beta' & \cos\phi \sin\beta' \\ \sin\phi \sin\beta' & 0 \end{pmatrix}
\tag{12}
$$

$$
\underline{\underline{N}}_{A_4} = \frac{1}{\sqrt{1 - (\sin\phi' \sin\beta')^2}} \begin{pmatrix} -\cos\beta' & -\cos\phi' \sin\beta' \\ -\cos\phi' \sin\beta' & \cos\beta' \end{pmatrix}
\tag{13}
$$

$$
\underline{\underline{N}}_{A_5} = \begin{pmatrix} 0 & (1 - R_{\perp_0}) \sin \phi' \sin \beta' \\ 1 + R_{\|_0} & 0 \end{pmatrix} \tag{14}
$$

$$
\underline{\underline{N}}_{A_6} = \begin{pmatrix} (1 - R_{\|_0}) \sin \phi' \sin \beta' & 0 \\ 0 & -(1 + R_{\perp_0}) \end{pmatrix} \tag{15}
$$

$$
\underline{\underline{N}}_{A_7} = \frac{1}{\sqrt{1 - (\sin \phi' \sin \beta')^2}} \begin{pmatrix} \sin \phi' \cos \beta' & \cos \phi' \\ -\cos \phi' & \sin \phi' \cos \beta' \end{pmatrix} \tag{16}
$$

$$
\underline{\underline{N}}_{B_1} = \underline{\underline{N}}_{A_1} \tag{17}
$$

$$
\underline{\underline{N}}_{B_2} = \begin{pmatrix} 1 - (\cos \phi \sin \beta')^2 & -\sin \phi \cos \phi \sin^2 \beta' & -\cos \phi \sin \beta' \cos \beta' \\ -\sin \phi \cos \phi \sin^2 \beta' & 1 - (\sin \phi \sin \beta')^2 & -\sin \phi \sin \beta' \cos \beta' \\ -\cos \phi \sin \beta' \cos \beta' & -\sin \phi \sin \beta' \cos \beta' & \sin^2 \beta' \end{pmatrix} \tag{18}
$$

$$
\underline{\underline{N}}_{B_3} = \begin{pmatrix} 0 & \cos \beta' & -\sin \phi \sin \beta' \\ -\cos \beta' & 0 & \cos \phi \sin \beta' \\ \sin \phi \sin \beta' & -\cos \phi \sin \beta' & 0 \end{pmatrix} \tag{19}
$$

$$
\underline{\underline{N}}_{B_4} = \frac{1}{\sqrt{1 - [\sin(n\pi - \phi') \sin \beta']^2}} \begin{pmatrix} \cos(n\pi) \cos \beta' & -\cos(n\pi) \cos(n\pi - \phi') \sin \beta' \\ \sin(n\pi) \cos \beta' & -\sin(n\pi) \cos(n\pi - \phi') \sin \beta' \\ \cos(n\pi - \phi') \sin \beta' & \cos \beta' \end{pmatrix} \tag{20}
$$

$$
\underline{\underline{N}}_{B_5} = \begin{pmatrix} 0 & (1 - R_{\perp_{n\pi}}) \sin(n\pi - \phi') \sin \beta' \\ 1 + R_{\|_{n\pi}} & 0 \end{pmatrix} \tag{21}
$$

$$
\underline{\underline{N}}_{B_6} = \begin{pmatrix} (1 - R_{\|_{n\pi}}) \sin(n\pi - \phi') \sin \beta' & 0 \\ 0 & -1 - R_{\perp_{n\pi}} \end{pmatrix} \tag{22}
$$

$$
\underline{\underline{N}}_{B_7} = \frac{1}{\sqrt{1 - [\sin(n\pi - \phi') \sin \beta']^2}} \begin{pmatrix} \sin(n\pi - \phi') \cos \beta' & -\cos(n\pi - \phi') \\ \cos(n\pi - \phi') & \sin(n\pi - \phi') \cos \beta' \end{pmatrix} \tag{23}
$$

4. Numerical Examples

Two sets of figures are shown in Section 4 to prove the effectiveness of the UAPO-based method for evaluating the electromagnetic scattering from an arbitrary-angled PEC wedge that is covered by a DNG MTM uniform layer. One should note that no limitations exist for the values of permittivity and permeability. The first set (Figures 2–5) is devoted to the ability of the UAPO diffracted field to compensate for the jumps of the GO field at the shadow boundaries, whereas the second set (Figures 6–10) includes comparisons with the Comsol Multiphysics® data. Both sets refer to a composite wedge that is characterized by $\alpha = 135°$ ($n = 1.25$), $\varepsilon_r = -(3.2 + j0.08)$, $\mu_r = -(8 + j0.09)$, and $d = 0.1\lambda_0$ if λ_0 is the free-space wavelength. Moreover, P moves on a circular arc with $\rho = 6\lambda_0$ and, according to the α value, ϕ varies from 0 to 225°.

The magnitudes of the $\beta-$ and $\phi-$ components of the GO field, the UAPO diffracted field, and the total field are reported in Figures 2 and 3, respectively, where $\beta' = 70°$, $\phi' = 80°$. Both of the wedge surfaces are lit by the incident wave ($U_{0,n\pi} = 1$) so that two reflection boundaries exist at $\phi = 100°, 190°$, where the GO field fails and exhibits inacceptable jumps. As expected, the UAPO diffracted field assumes significant magnitude values in the angular regions around such directions, and it is able to balance the GO jumps, so offering a continuous total field from 0 to 225°. This ability is due to the behavior of the diffraction contribution at the shadow boundaries: the value on the left side is different from the value on the right side, so obtaining the needed discontinuity for the compensation. Figures 4 and 5, which refer to $\beta' = 70°, \phi' = 40°$ also confirm such an ability when one reflected field boundary ($\phi = 140°$) and one incident field boundary ($\phi = 220°$) exist since the incident wave impacts only one surface ($U_0 = 1$, $U_{n\pi} = 0$).

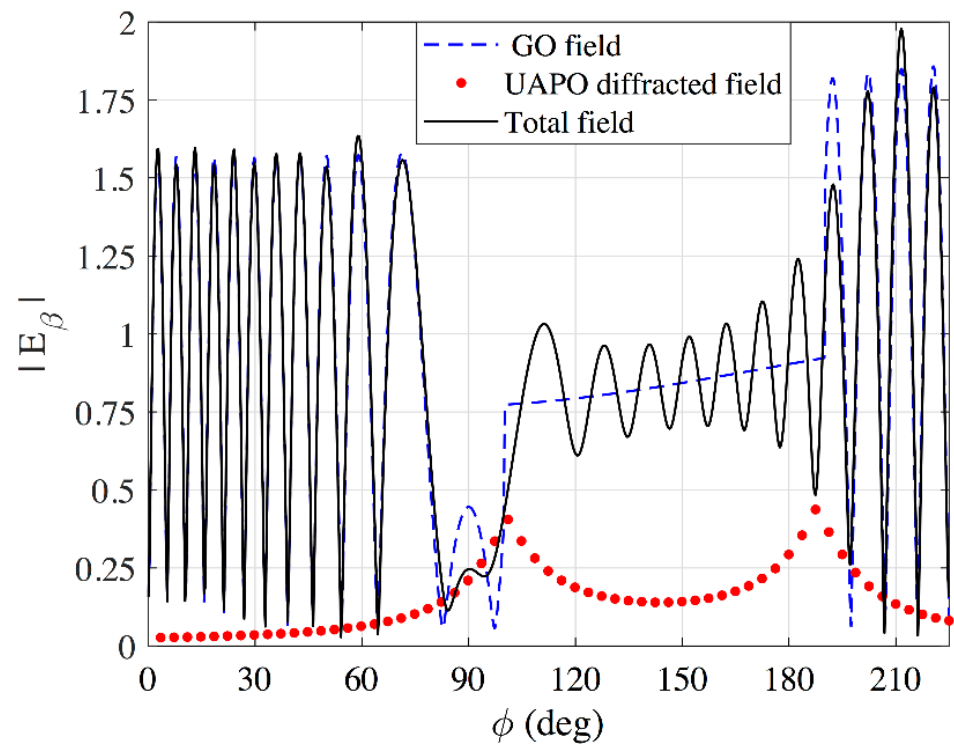**Figure 2.** Modulus of the β-components with $\beta' = 70°, \phi' = 80°, E_{\beta'}^i = 1, E_{\phi'}^i = 0$.

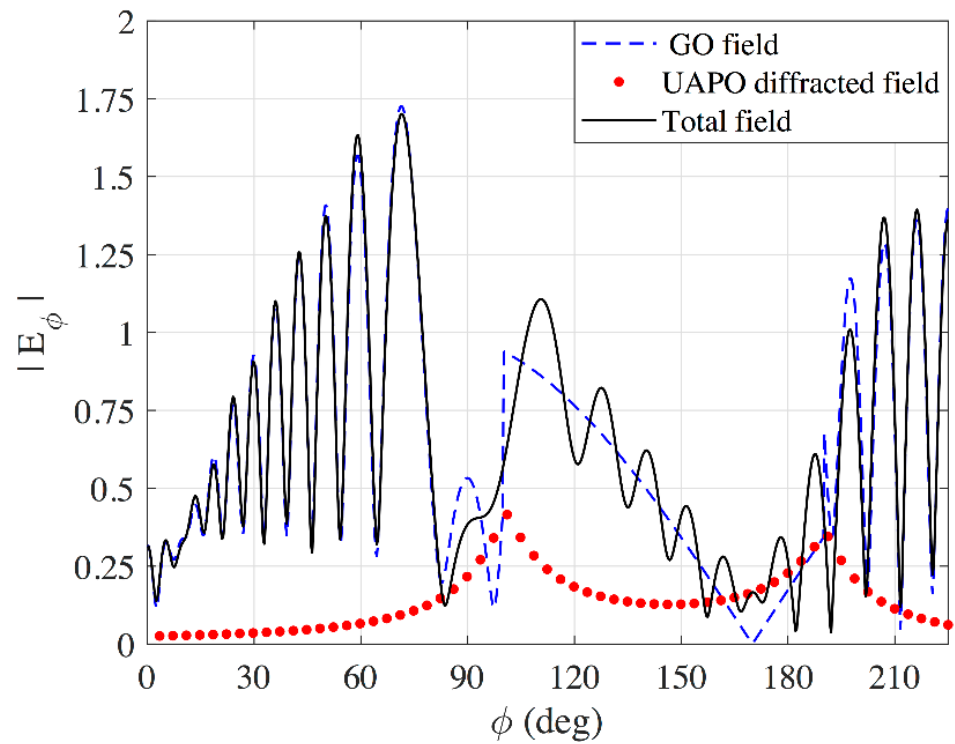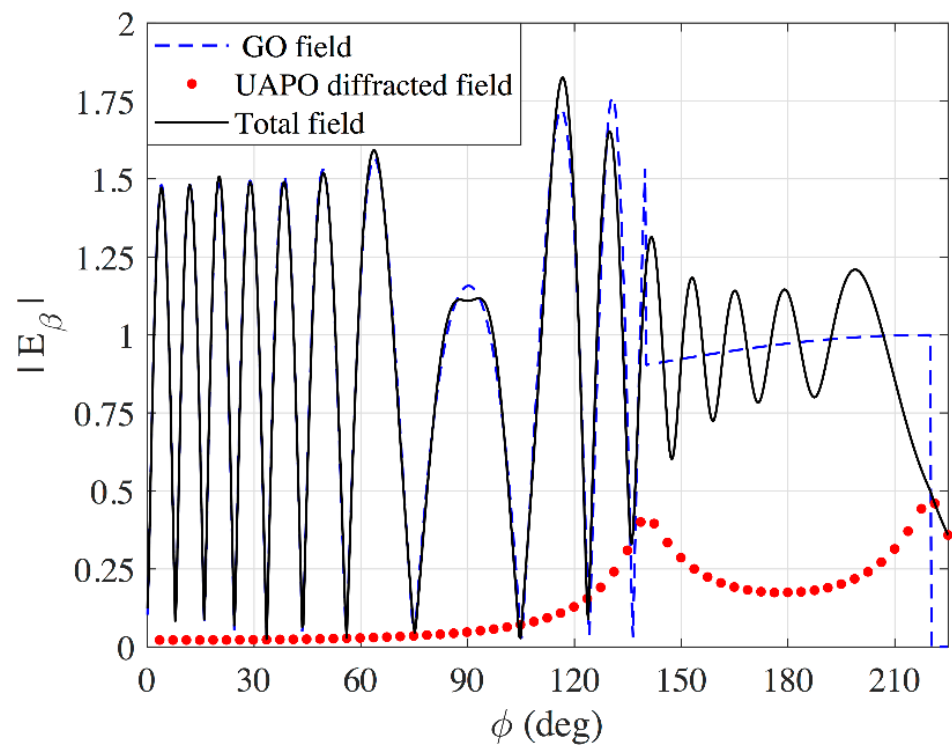**Figure 3.** Modulus of the φ-components with $\beta' = 70°, \phi' = 80°, E_{\beta'}^i = 0, E_{\phi'}^i = 1$.

Figure 4. Modulus of the β-components with $\beta' = 70°, \phi' = 40°, E_{\beta'}^i = 1, E_{\phi'}^i = 0$.

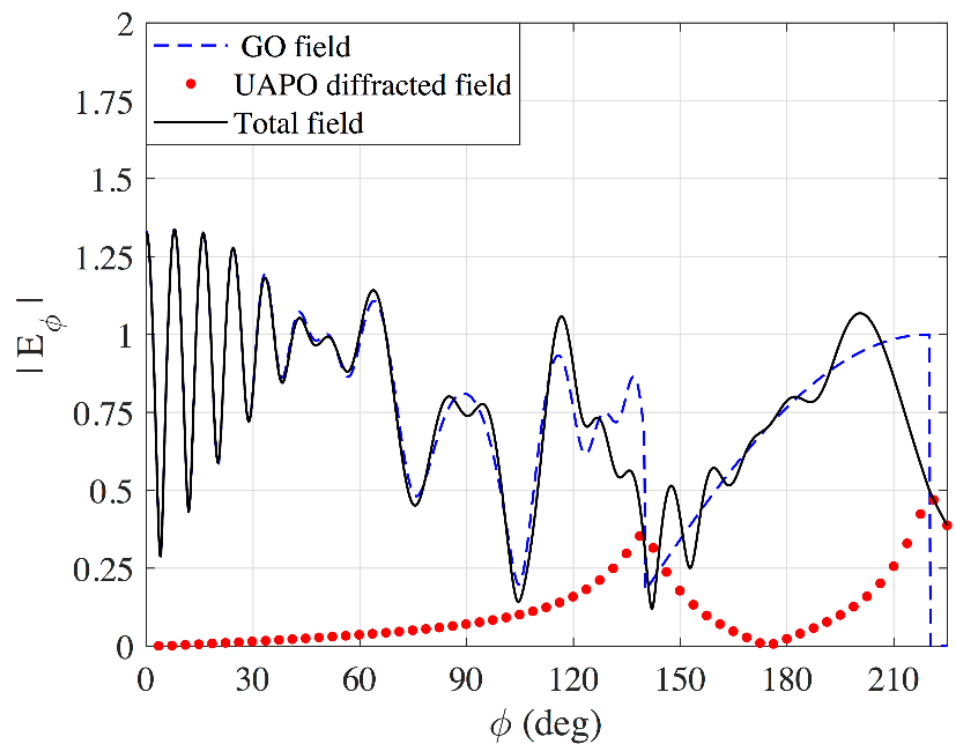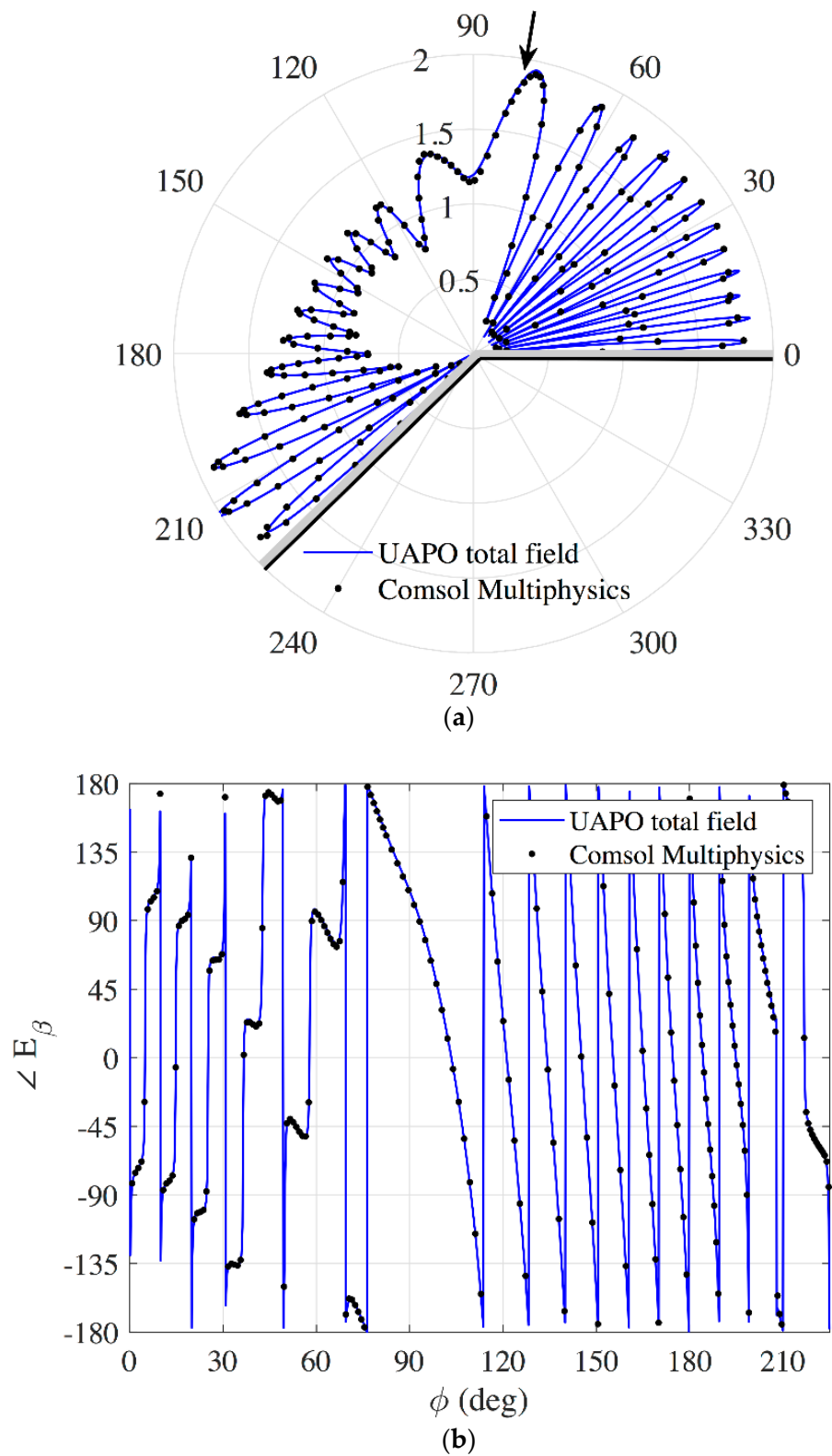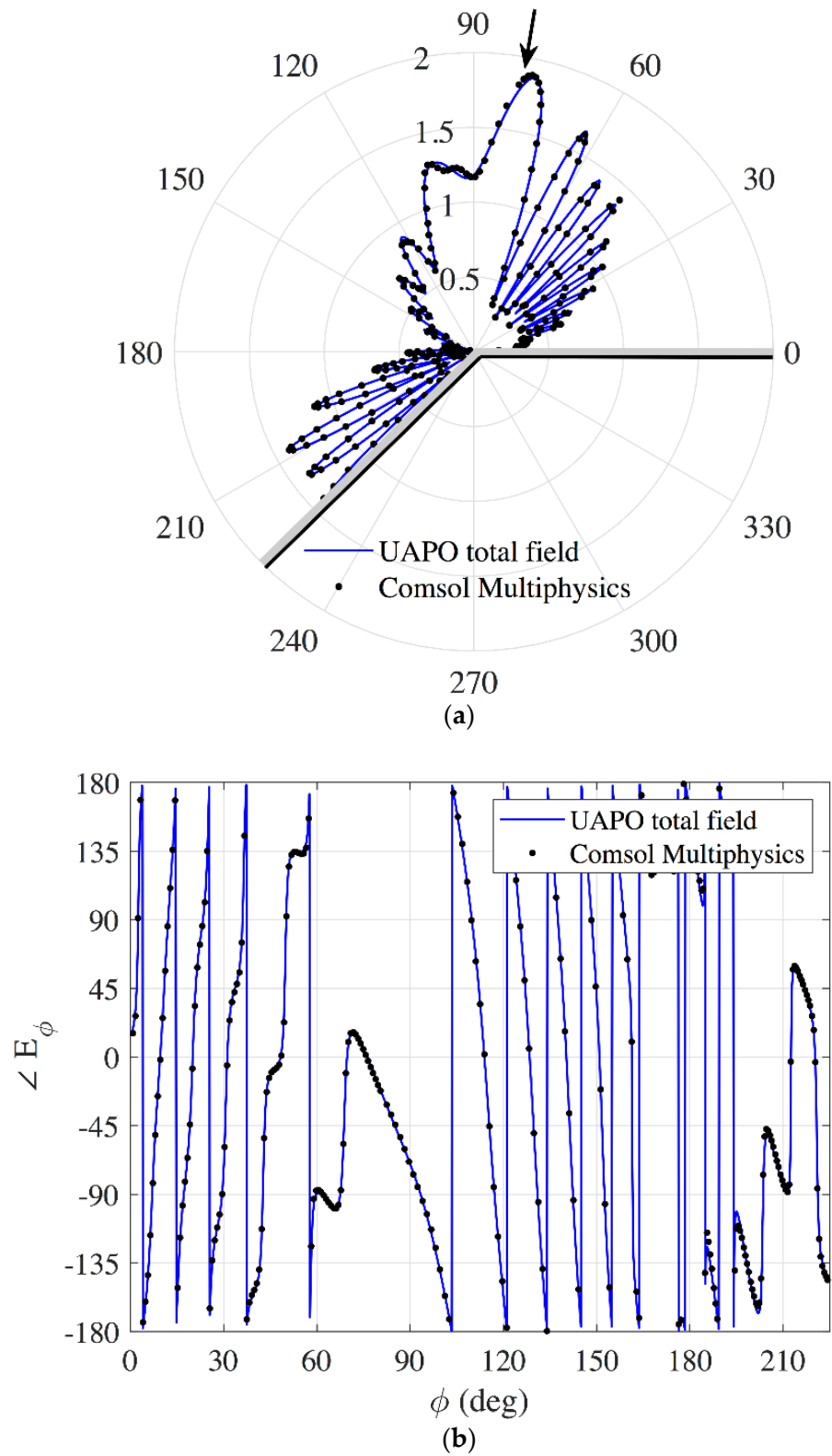**Figure 5.** Modulus of the φ-components with $\beta' = 70°, \phi' = 40°, E_{\beta'}^i = 0, E_{\phi'}^i = 1$.

(a)

(b)
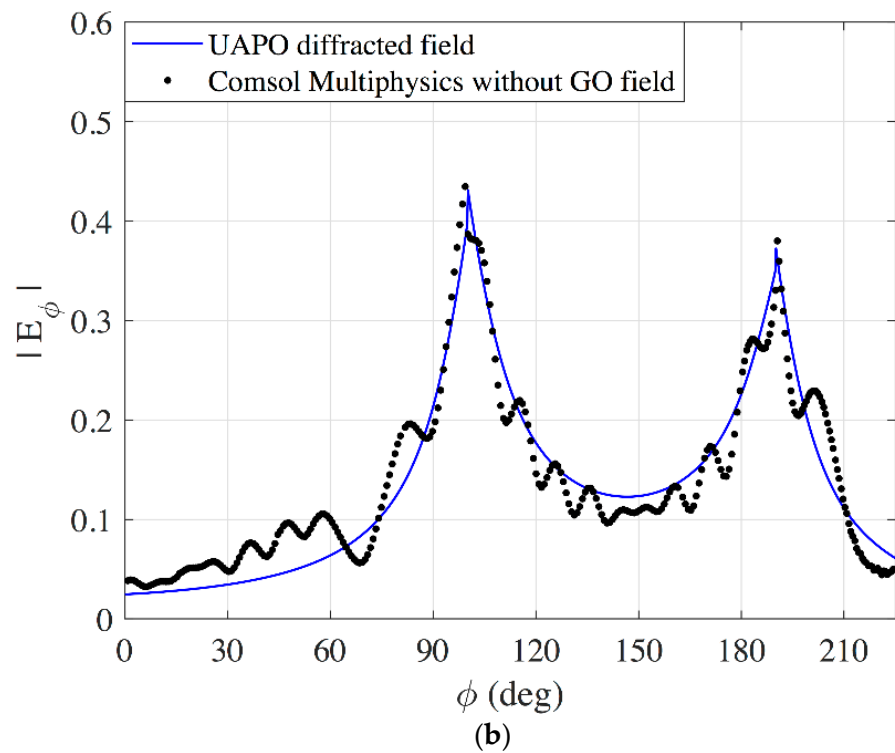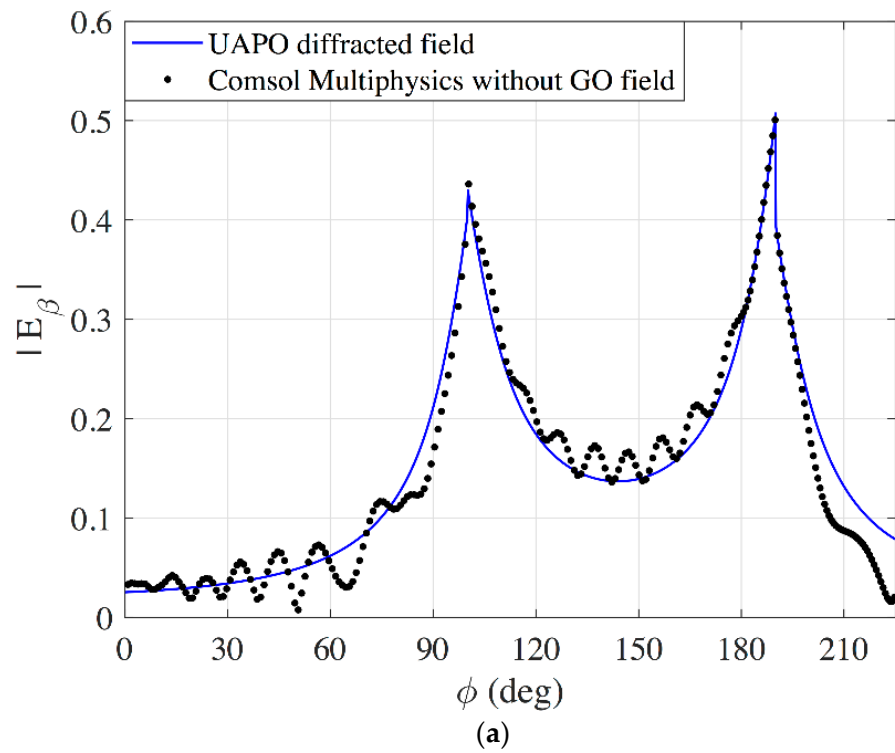
Figure 6. Test by using Comsol Multiphysics® output with $\beta' = 90°, \phi' = 80°, E^i_{\beta'} = 1, E^i_{\phi'} = 0$. (a) Modulus of the β-component. (b) Phase of the β-component.
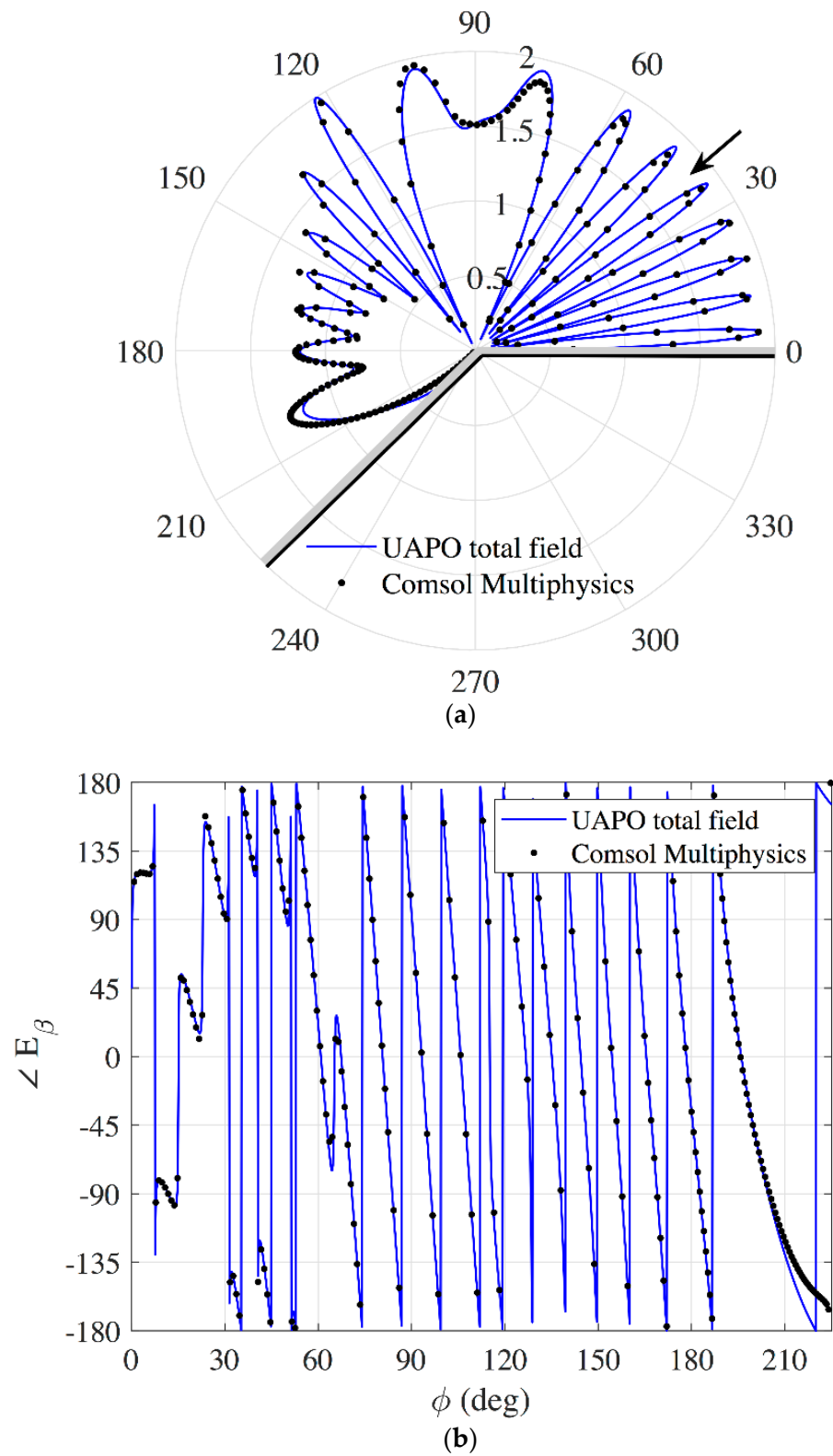
Figure 7. Test by using Comsol Multiphysics$^{®}$ output with $\beta' = 90°, \phi' = 80°, E^i_{\beta'} = 0, E^i_{\phi'} = 1$. (**a**) Modulus of the φ-component. (**b**) Phase of the φ-component.

(a)

(b)

Figure 8. Test by using Comsol Multiphysics® output with $\beta' = 90°, \phi' = 80°$. (a) Modulus of the β-component with $E^i_{\beta'} = 1, E^i_{\phi'} = 0$. (b) Modulus of the φ-component with $E^i_{\beta'} = 0, E^i_{\phi'} = 1$.

Figure 9. Test by using Comsol Multiphysics® output with $\beta' = 90°, \phi' = 40°, E^i_{\beta'} = 1, E^i_{\phi'} = 0$. (**a**) Modulus of the β-component. (**b**) Phase of the β-component.

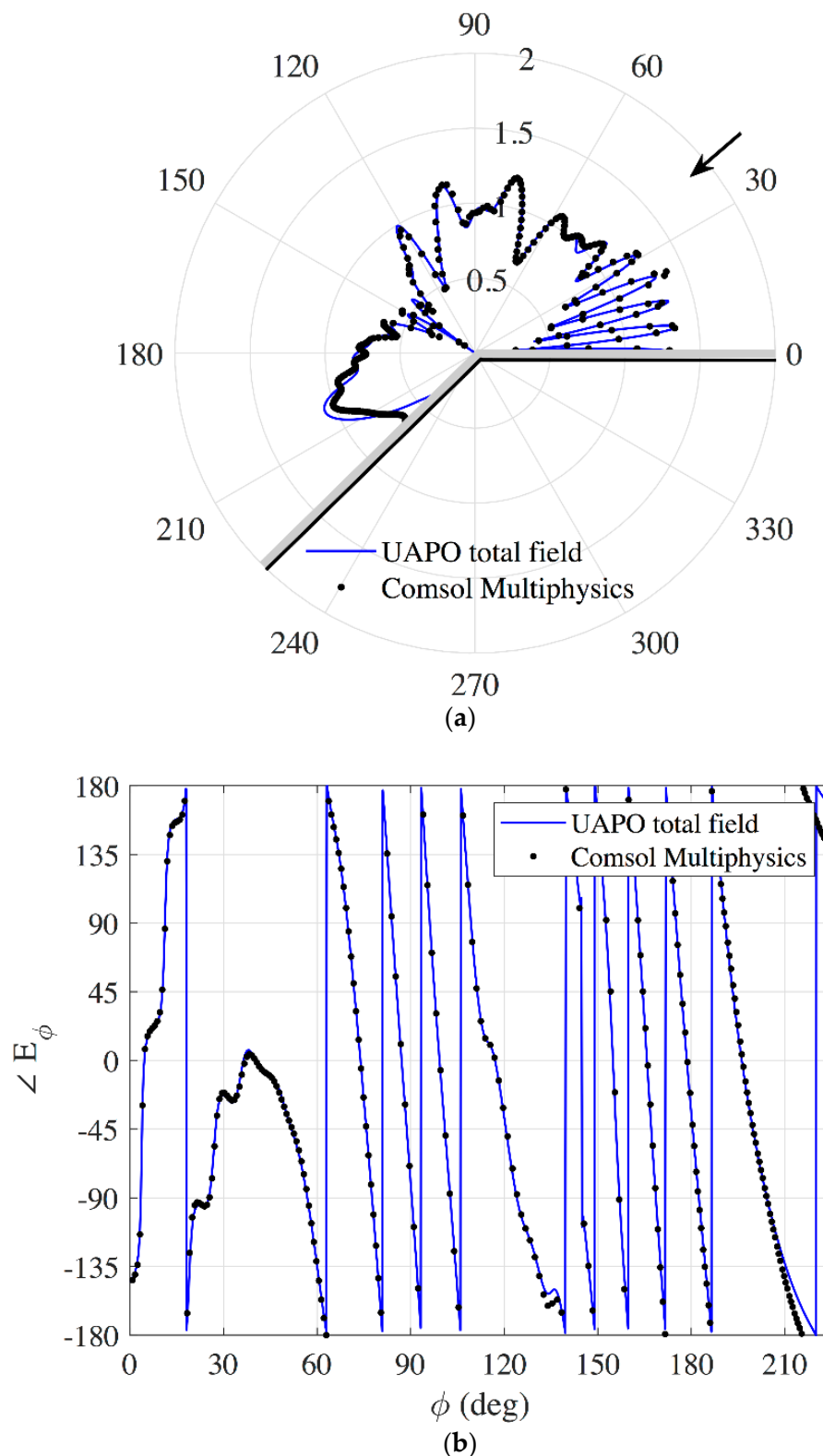**Figure 10.** Test by using Comsol Multiphysics® output with $\beta' = 90°, \phi' = 40°, E^i_{\beta'} = 0, E^i_{\phi'} = 1$. (**a**) Modulus of the φ-component. (**b**) Phase of the φ-component.

With reference to the figures of the second set, the wave propagation is considered to be orthogonal to the edge ($\beta' = 90°$) to reduce the needed computation effort when one is running the RF unit of Comsol Multiphysics®. The apex of the wedge is centered

in a square propagation scenario with the side length of $33.3\lambda_0$ and the thickness of the perfectly matched layer at the box boundary is $2\lambda_0$. In order to obtain reliable data, automatic adaptive meshes from $0.000075\lambda_0$ to $0.075\lambda_0$ have been used.

Save for Figure 8, the Figures from 6 to 10 contain: (a) the amplitude of the UAPO-based field component and the corresponding Comsol Multiphysics® data; (b) a comparison between the related phases. One should note that the reported plots show large fluctuations, so providing hard test-beds.

Figures 6 and 7 are relevant to $E^i_{\beta'} = 1, E^i_{\phi'} = 0$ and $E^i_{\beta'} = 0, E^i_{\phi'} = 1$, respectively, when $\phi' = 80°$, and despite the fast variability of amplitude and phase of the field, the UAPO-based data fit very well those attained by Comsol Multiphysics®. Moreover, the interested reader can surely appreciate Figure 8a,b, where the UAPO diffracted field components are compared with the corresponding Comsol Multiphysics® data that were obtained by extracting the GO field contributions. The agreements are very encouraging.

The last figures refer to $\phi' = 40°$. Accordingly, one surface of the wedge is involved in the evaluation of the UAPO diffracted field as in Figures 4 and 5. Good results are again achieved, but some of the lobes of the amplitude patterns are not correctly recovered and the phase values show misalignments in correspondence of the angular region centered on the incident field boundary. It is authors' opinion that such a case suffers from the absence of the diffraction contribution from the internal PEC wedge.

5. Conclusions

The UAPO approach has been applied to the evaluation of the diffraction contribution arising from the interaction of the plane waves and the arbitrary-angled metallic wedges that are covered by DNG MTM uniform layers. In particular, the three-dimensional problem has been solved in the case of skew incidence with respect to the edge, so overcoming the two-dimensional scheme in [1,2]. The UAPO diffracted field is again formulated in an explicit and easy-to-handle form, and this allows us to obtain total fields without performing jumps. Very good results have been attained when both of the wedge surfaces have been lit by the incident plane wave, whereas small inaccuracies have been revealed when one wedge surface has been shadowed by the wave direction. It is the authors' opinion that this is due to the absence of the diffraction contribution from the PEC wedge in the total field evaluation.

Author Contributions: Conceptualization, G.R.; Methodology, G.R.; Formal analysis, G.R.; Software, G.G. and F.F.; Validation, G.G., F.F. and R.G.; Writing—original draft preparation, G.R.; Writing—review and editing, G.R., G.G., F.F., C.G. and R.G. All authors have read and agreed to the published version of the manuscript.

Institutional Review Board Statement: Not applicable.

Informed Consent Statement: Not applicable.

Data Availability Statement: This statement must be excluded.

Conflicts of Interest: The authors declare no conflict of interest.

References

1. Gennarelli, G.; Riccio, G. A uniform asymptotic solution for the diffraction by an arbitrary-angled wedge coated by lossy DNG metamaterials: The case of normal incidence. In Proceedings of the 13th EUCAP, Krakow, Poland, 31 March–5 April 2019; pp. 2269–2272.
2. Riccio, G.; Gennarelli, G.; Ferrara, F.; Gennarelli, C.; Guerriero, R. Diffraction of plane waves by arbitrary-angled coated wedges. *Progr. Electromagn. Res. M* **2022**, *108*, 103–113. [CrossRef]
3. Kouyoumjian, R.G.; Pathak, P.H. A uniform geometrical theory of diffraction for an edge in a perfectly conducting surface. *Proc. IEEE* **1974**, *62*, 1448–1461. [CrossRef]
4. Riccio, G.; Gennarelli, G.; Ferrara, F.; Gennarelli, C.; Guerriero, R. Diffraction by a right-angled metallic wedge with coating: The UAPO solution for normal incidence. *Int. J. Microw. Opt. Technol.* **2022**, *17*, 196–202.

5. Engheta, N.; Ziolkowski, R.W. (Eds.) *Metamaterials: Physics and Engineering Explorations*; John Wiley & Sons Inc.: Hoboken, NJ, USA, 2006.

6. Marquéz, R.; Martin, F.; Sorolla, M. *Metamaterials with Negative Parameters: Theory, Design and Microwave Applications*; John Wiley & Sons Inc.: Hoboken, NJ, USA, 2008.

7. Sakoda, K. (Ed.) *Electromagnetic Metamaterials: Modern Insights into Macroscopic Electromagnetic Fields*; Springer: Singapore, 2019.

8. Bilotti, F.; Sevgi, L. Metamaterials: Definitions, properties, applications, and FDTD-based modeling and simulation. *Int. J. RF Microw. Comput. Aided Eng.* **2012**, *22*, 422–438. [CrossRef]

9. Singh, G.; Rajni; Marwaha, A. A review of metamaterials and its applications. *Int. J. Eng. Trends Technol.* **2015**, *19*, 305–310. [CrossRef]

10. Bukhari, S.S.; Vardaxoglou, J.; Whittow, W. A metasurfaces review: Definitions and applications. *Appl. Sci.* **2019**, *9*, 2727. [CrossRef]

11. Xiao, S.; Wang, T.; Liu, T.; Zhou, C.; Jiang, X.; Zhang, J. Active metamaterials and metadevices: A review. *J. Phys. D Appl. Phys.* **2020**, *53*, 503002. [CrossRef]

12. Suresh Kumar, N.; Naidu, K.C.B.; Banerjee, P.; Anil Babu, T.; Venkata Shiva Reddy, B. A review on metamaterials for device applications. *Crystal* **2021**, *11*, 518. [CrossRef]

13. Gennarelli, G.; Riccio, G. Diffraction by a planar metamaterial junction with PEC backing. *IEEE Trans. Antennas Propag.* **2010**, *58*, 2903–2908. [CrossRef]

14. Riccio, G.; Gennarelli, G.; Ferrara, F.; Gennarelli, C.; Guerriero, R. Scattering from a truncated metamaterial layer hosted by a planar PEC structure: Uniform asymptotic solution and validation tests. *Appl. Sci.* **2022**, *12*, 7302. [CrossRef]

15. Gennarelli, G.; Riccio, G. A uniform asymptotic solution for diffraction by a right-angled dielectric wedge. *IEEE Trans. Antennas Propag.* **2011**, *59*, 898–903. [CrossRef]

16. Gennarelli, G.; Riccio, G. Diffraction by 90° penetrable wedges with finite conductivity. *J. Opt. Soc. Am. A* **2014**, *31*, 21–25. [CrossRef] [PubMed]

17. Frongillo, M.; Gennarelli, G.; Riccio, G. Diffraction by a structure composed of metallic and dielectric 90° blocks. *IEEE Antennas Wireless Propag. Lett.* **2018**, *17*, 881–885. [CrossRef]

18. Frongillo, M.; Gennarelli, G.; Riccio, G. Plane wave diffraction by arbitrary-angled lossless wedges: High-frequency and time-domain solutions. *IEEE Trans. Antennas Propag.* **2018**, *66*, 6646–6653. [CrossRef]

19. Gennarelli, G.; Frongillo, M.; Riccio, G. High-frequency evaluation of the field inside and outside an acute-angled dielectric wedge. *IEEE Trans. Antennas Propag.* **2015**, *63*, 374–378. [CrossRef]

20. Frongillo, M.; Gennarelli, G.; Riccio, G. TD-UAPO diffracted field evaluation for penetrable wedges with acute apex angle. *J. Opt. Soc. Am. A* **2015**, *32*, 1271–1275. [CrossRef] [PubMed]